

Latent Processes Identification From Multi-View Time Series

Zenan Huang^{1,4}, Haobo Wang⁴, Junbo Zhao⁴ and Nenggan Zheng^{*1,2,3,4}

¹Qiushi Academy for Advanced Studies (QAAS), Zhejiang University

²the State Key Lab of Brain-Machine Intelligence, Zhejiang University

³CCAI by MOE and Zhejiang Provincial Government (ZJU)

⁴College of Computer Science and Technology, Zhejiang University

{lcurious, wanghaobo, j.zhao, zng}@zju.edu.cn,

Abstract

Understanding the dynamics of time series data typically requires identifying the unique latent factors for data generation, *a.k.a.*, latent processes identification. Driven by the independent assumption, existing works have made great progress in handling single-view data. However, it is a non-trivial problem that extends them to multi-view time series data because of two main challenges: (i) the complex data structure, such as temporal dependency, can result in violation of the independent assumption; (ii) the factors from different views are generally overlapped and are hard to be aggregated to a complete set. In this work, we propose a novel framework MuLTI that employs the contrastive learning technique to invert the data generative process for enhanced identifiability. Additionally, MuLTI integrates a permutation mechanism that merges corresponding overlapped variables by the establishment of an optimal transport formula. Extensive experimental results on synthetic and real-world datasets demonstrate the superiority of our method in recovering identifiable latent variables on multi-view time series.

1 Introduction

Detecting causal relationships from time series based on observations is a challenging problem in many fields of science and engineering [Spirites *et al.*, 2000]. A thorough grasp of causal relationships, interaction pathways, and time lags is valuable for interpreting and modeling temporal processes [Pearl, 2000]. Existing works [Chickering, 2002; Tsamardinos *et al.*, 2006; Zhang, 2008; Hoyer *et al.*, 2008; Zheng *et al.*, 2018] typically rely on predefined variables. However, such a strategy is not directly applicable to real-world scenarios, where data are intertwined with unknown generation processes, and causal variables are not readily available. Therefore, identifying the latent sources is crucial for interpreting underlying causal relations and elucidating the genuine dynamics inherent in the temporal data.

*Corresponding author.

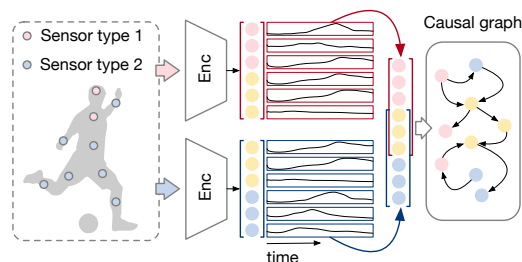


Figure 1: The diagram depicts a pipeline analyzing multi-view physiological time-series data. This pipeline learns temporal embeddings from both views, aligns variables considering their dependencies, and effectively reveals underlying variables and relationships.

To cope with this problem, non-linear independent component analysis (nICA) [Hyvärinen and Pajunen, 1999] has shown promising results in terms of identifiability, by effectively exploiting the underlying structure of the data. On time series data, most nICA techniques attempt to utilize the temporal structure among sequential observations, such as temporal contrastive learning [Hyvärinen and Morioka, 2016], permutation contrastive learning [Hyvärinen and Morioka, 2017], and generalized contrastive learning [Hyvärinen *et al.*, 2019]. However, these methods inherently assume the latent components are independent, which may not hold in practice. Moreover, in broader real-world scenarios, causal discovery tasks mostly require identifying dependent relations from extensive data collections, which may further restrict the identifiability of nICA techniques. Take Figure 1 as an example, understanding the physiological processes of human actions requires jointly analyzing the data across multiple kinds of sensors and a physiological signal may influence multiple downstream regions with different time lags. Similar cases also exist in a wide variety of real-world scenarios, such as multi-view sensors information fusion [He *et al.*, 2021], multi-market stock index analysis [Wang *et al.*, 2020], *etc.* Hitherto, few efforts have been made to address such challenging yet realistic problems.

The example above, which we call the multi-view latent process identification (MVLPI) problem, poses two combinatorial challenges. First, the diverse time delays in interactions among variables in time series data complicate direct estimation of latent variables. Second, different views typically

correlate with subsets of latent factors. Due to identifiability issues, merely inverting these views does not guarantee alignment of the recovered factors. Hence, aggregating them to the final complete latent variables is non-trivial.

In this paper, we propose the **Multi-view Latent Processes Identification** (dubbed **MuLTI**) framework that learns identifiable causal related variables from the multi-view data. MuLTI identifies latent variables from multi-view observations using three strategies: 1) It reformulates causally related process distributions using conditional independence, replacing original latent variables with independent causal process noises; 2) It applies contrastive learning to maximize mutual information between prior and posterior conditional distributions; 3) It aligns partially overlapping latent variables using learnable permutation matrices, optimized with Sinkhorn method. The first two strategies ensure the learning of identifiable latent variables, while the last one bridges the causal relations across multiple views. Given that only a subset of each view’s source components correspond, matching and merging shared latent variables resemble the sorting and alignment of top-k shared components among estimated variables.

We evaluate our method on both synthetic and real-world data, spanning multivariable time series and visual tasks. Experiment results show that the latent variables are reliably identified from observational multi-view data. To the best of our knowledge, the learning of causal dependent latent variables from multi-view data has no prior solution. The proposed framework may also serve as a factor analyzing tool for extracting reliable features for downstream tasks of multi-view learning. More theoretical and empirical results can be found in Appendix.

2 Methodology

2.1 Problem Formulation

In contrast to the single-view setup, the MVLPI problem presents a unique challenge: only a portion of the latent factors can be recovered from an individual view. Thus, it is necessary to revisit the data-generating procedure of the MVLPI task. As shown in Figure 2, we consider the MVLPI task on the time series data, with the goal of recovering the latent factor $\mathbf{z}_t \in \mathbb{R}^d$ at each time step t , which uniquely generates the observed views. To achieve this, we make a common assumption that the current state is spatiotemporally dependent on the historical states,

$$\mathbf{z}_{i,t} = f_i(\mathbf{Pa}(z_{i,t}), \epsilon_{i,t}), \quad (1)$$

where $\mathbf{Pa}(z_{i,t})$ denotes causal parents of i -th factor at current step t , $\epsilon_{i,t}$ denotes a noise component of causal transition. While \mathbf{z}_t contains a complete set of latent factors that we are truly interested in, we note that each observed view may be dependent on only a subset of it. Formally, we have the following data-generating process,

$$\mathbf{x}_t^1 = g^1(\mathbf{z}_t^1), \quad \mathbf{x}_t^2 = g^2(\mathbf{z}_t^2), \quad \text{where } \mathbf{z}_t = \mathbf{z}_t^1 \cup \mathbf{z}_t^2, \quad (2)$$

where \mathbf{x}_t^v is the v -th observed view at time step t , and $g^v(\cdot)$ is the corresponding map function. Note that here we consider a 2-view setup for the sake of brevity, while our framework can be easily generalized to handle more views.

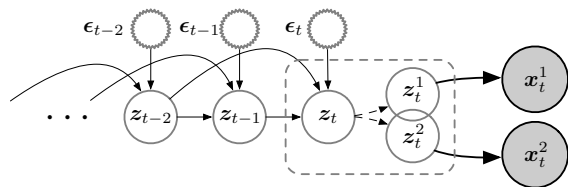


Figure 2: Graphical model of data generation. Each view may be generated by part of latent variables individually.

Following the above definition, we can identify the factors from the observed views, and aggregate them into the complete version \mathbf{z}_t . However, as each view performs a distinctive nonlinear mixing of the source factors, it is challenging to identify the corresponding latent variables entangled in views, or to ensure the factors from different views are in the same subspace. Second, though we slightly abuse the notation ‘ \cup ’ to show the *aggregation* relation of view-specific and the complete factors, it is non-trivial to reconstruct the complete \mathbf{z}_t from a set of indeterminate estimations in practice. To remedy this problem, we introduce our novel **MuLTI** framework which comprises a contrastive learning module for enhanced identifiability alongside a novel merge operator that aggregates the view-specific latent variables to a complete one. The whole procedure is illustrated in Figure 3.

2.2 Contrastive Learning Module

Our goal is to learn an inverse function $r(\cdot)$ from the observed data. This is achieved by: (1) individually inverting functions $\{r^v(\cdot)\}$; (2) a merge function $m : \{\mathcal{Z}^v\} \mapsto \mathcal{Z}$, in a way that $r(\cdot) = m(\{r^v(\mathbf{x}^v)\})$. Note that each $r^v(\cdot)$ corresponds to an inverse of $g^v(\cdot)$, and the reverse function $r(\cdot)$ parameterizes the distribution of $q_r(\mathbf{z}_t | \{\mathbf{x}_t^v\})$. The merge operator will be introduced in the next section. The following paragraphs will describe the identification procedure of \mathbf{z}_t . Formally speaking, there exists an indeterminacy mapping $h = r \circ g$ between estimated $\tilde{\mathbf{z}}_t = h(\mathbf{z}_t)$ and true \mathbf{z}_t . The goal is to identify the true value of \mathbf{z}_t . We exploit the spatiotemporal dependencies of \mathbf{z}_t to infer the values of latent variables from preceding states, as shown in Eq.(1). To achieve this, we introduce the causal transition function $f(\cdot)$ to parameterize the conditional distribution $q_{f,h}(\mathbf{z}_t | \mathbf{z}_{H_t})$, where \mathbf{z}_{H_t} denotes the set of preceding states of \mathbf{z}_t . Empirically, we estimate an alternative value of the complete latent factor by $\tilde{\mathbf{z}}_t = f(\mathbf{z}_{H_t})$.

Motivated by the results of nICA [Hyvärinen *et al.*, 2019; Zimmermann *et al.*, 2021], we can identify the underlying factors of data with a certain low indeterminacy by carefully exploiting the inherent structure of data via a variety of conditional distributions. To this end, we can achieve model identifiability - that is, the ability to exactly recover the variables \mathbf{z}_t and their associated causal relations - by learning the function r , in such a way as to ensure h is an isometry. Specifically, $h : \mathcal{Z} \mapsto \mathcal{Z}$ must satisfy the condition $\delta(\mathbf{z}_t, \tilde{\mathbf{z}}_t) = \delta(h(\mathbf{z}_t), h(\tilde{\mathbf{z}}_t))$ everywhere, where $\delta(\cdot, \cdot)$ is a metric. Using the conditional dependency in sequential latent states $\{\mathbf{z}_t\}$, a key insight is to estimate the function f for causal relations modeling and estimate reverse function r :

$$\max_{r,f} \mathcal{I}(\tilde{\mathbf{z}}_t; \mathbf{z}_t) = \mathcal{I}(f(\mathbf{z}_{H_t}, \epsilon_t); \mathbf{z}_t), \quad (3)$$

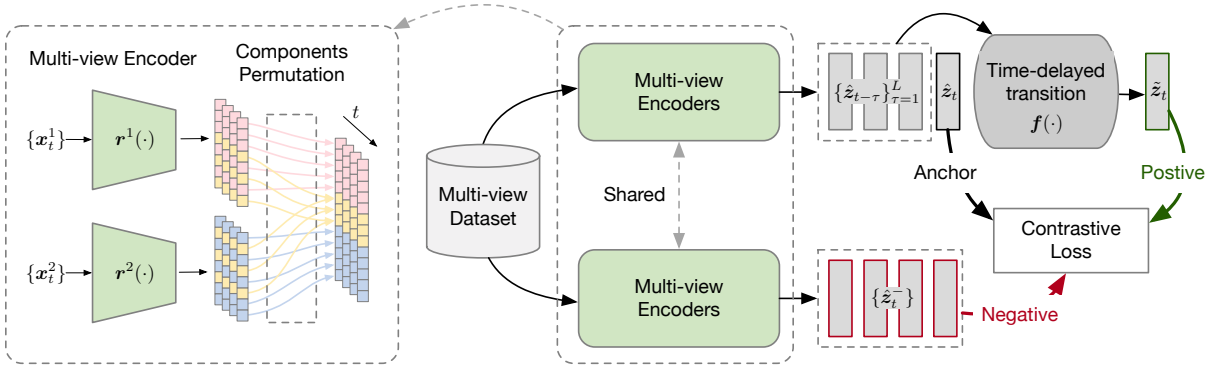


Figure 3: Illustration of our MuLTI framework. On one hand, we recover the view-specific latent factors \hat{z}_t^v from individual views, which are then merged to obtain \hat{z}_t . On the other hand, we exploit the temporal dependency to obtain a causal transition latent factor \tilde{z}_t from previously estimated \hat{z}_t . Thereafter, we regard them as positive pairs to optimize the contrastive loss, which serves as a surrogate of mutual information maximization to achieve identifiability.

where $\tilde{z}_t = f(z_{H_t}, \epsilon_t)$ is the estimated latent variable based on the previous latent variables z_{H_t} , $\mathcal{I}(\cdot, \cdot)$ indicates the mutual information. We denote the prior distribution as $p(\tilde{z}_t|z_{H_t})$ and the modeled distribution as $q_{h,f}(\tilde{z}_t|z_{H_t})$. The optimization problem defined in Eq. (3) can also be viewed as a minimization problem for the cross-entropy $H(\cdot||\cdot)$,

$$\min_{f,r} H(p(\tilde{z}_t|z_{H_t})||q_{f,r}(\tilde{z}_t|z_{H_t})). \quad (4)$$

Nevertheless, directly optimizing the Eq. (4) is typically difficult. To this end, we employ contrastive learning as a surrogate, given that it has been proven to be a variational bound of mutual information maximization [van den Oord *et al.*, 2018]. Formally, the contrastive loss is defined as follows,

$$\mathcal{L}_{\text{contr}}(r, f; \mu, M) := \mathbb{E}_{\substack{(\mathbf{x}, \tilde{\mathbf{x}}) \sim p_{\text{pos}} \\ \{\mathbf{x}_i^-\}_{i=1}^M \stackrel{i.i.d.}{\sim} p_{\text{data}}}} \left[-\log \frac{e^{-\delta(\mathbf{z}, \tilde{\mathbf{z}})/\mu}}{e^{-\delta(\mathbf{z}, \tilde{\mathbf{z}})/\mu} + \sum_{i=1}^M e^{-\delta(\mathbf{z}, \mathbf{z}_i^-)/\mu}} \right], \quad (5)$$

$M \in \mathbb{Z}_+$ represents the fixed number of negative samples, p_{data} denotes the distribution of all observations, and p_{pos} signifies the distribution of positive pairs, we choose the ℓ_1 as the metric, represented by $\delta(\cdot, \cdot)$, $\mu \geq 0$ represents the temperature. Here, we omit the subscript t for simplicity.

As mentioned earlier, we can infer the latent variable z_t in two ways: directly, with $\hat{z}_t = r(\{x_t^v\})$, and indirectly, with $\tilde{z}_t = f(z_{H_t})$. Given the expectation that these two inferred variables should be similar, we define the pair (\hat{z}_t, \tilde{z}_t) as a positive pairs. Subsequently, we sample data from the marginal distribution of observations, recover latent variables z_t^- , and form negative pairs with \hat{z}_t . At this point, the contrastive learning minimizes the cross-entropy between the ground-truth latent conditional distribution $p(z_t|z_{H_t})$ and a specific model distribution $q_{r,h}(z_t|z_{H_t})$. Thus, we have $\delta(h(z_t), h(f(z_{H_t}))) \propto \delta(z_t, f(z_{H_t}))$ for all z_t and $f(z_{H_t})$. This implies that the ground-truth z_t lies in the isometric space of the estimated \hat{z}_t , and can be further recovered through simple transformations.

2.3 Parametric causal transitions

To represent the causal transition process of $f(\cdot)$, we consider a widely-used parametric formulation that aligns well with the Granger causality [Ding *et al.*, 2006]. To parameterize the dependence of $z_{i,t}$ on its causal parents $\mathbf{Pa}(z_{i,t})$ in Eq. (1), we model the causal transition as following vector autoregressive (VAR) process. Let $\mathbf{A}_\tau \in \mathbb{R}^{d \times d}$ be the full rank state transition matrix at lag τ . Assuming the true z_t is known, the causal transition can be represented as follow,

$$z_t = f(z_{H_t}, \epsilon_t) = \sum_{\tau=1}^L \mathbf{A}_\tau z_{t-\tau} + \epsilon_t, \quad (6)$$

here, L is max time lag, ϵ_t is an additive noise variable. Using this formulation, we can reformulate the conditional distribution $p(z_t|z_{H_t})$ by changing the variables:

$$p(z_t|z_{H_t}) = p(z_t - \sum_{\tau=1}^L \mathbf{A}_\tau z_{t-\tau} = \epsilon_t). \quad (7)$$

As the ground-truth z_t is not readily available, we reuse the estimated \hat{z}_t to calculate Eq.(6). Through this reformulation, we can represent the causal transition using a mutually independent noise distribution.

Through the above proper definitions of the contrastive pairs and the causal transition f , minimizers of contrastive loss determine the h up to an isometry:

Theorem 1 (Minimizers of contrastive objective recover the latent variables and their relations). *Let latent space \mathcal{Z} be a convex body in \mathbb{R}^d , $h = r \circ g : \mathcal{Z} \mapsto \mathcal{Z}$, f be a causal transition function, and δ be a metric, induced by a norm. If g is differentiable and injective, r, f are expressive enough to be minimizers of contrastive objective $\mathcal{L}_{\text{contr}}$ in Eq. (5) for $M \rightarrow +\infty$, then, we have $h = r \circ g$ is invertible and affine mapping and f captures the ground-truth causal relations.*

Theorem 1 guarantees the identifiability of the encoder r and causal transition function f . Specifically, the contrastive loss enforces $\delta(h(\hat{z}_t), h(z_t)) \propto \delta(\hat{z}_t, z_t)$ almost everywhere, which leads h to be an isometry, *i.e.*, there exists an orthogonal matrix $\mathbf{U} \in \mathbb{R}^{d \times d}$ such that $\hat{z}_t = \mathbf{U}z_t$ and $\hat{\mathbf{A}}_\tau = \mathbf{A}_\tau \mathbf{U}^\top$. Further, when ϵ_t is non-Gaussian (*e.g.*, Laplacian), and metric $\delta(\cdot, \cdot)$ is non-isotropic (*e.g.*, ℓ_1 norm), there is only a chan-

nel permutation π between estimations and ground-truth such that $\hat{z}_{i,t} = s_i z_{\pi(i),t}$, where s_i is a scaling constant.

2.4 Merge Operation

As mentioned earlier, a significant challenge in learning a spatiotemporal dependent source from multi-view data lies in aggregating the view-specific source, z_t^v , into the complete latent source, z_t . This is because each view only holds a portion of the total information. Given that sources estimated from each view exhibit unique uncertainties, ensuring their alignment within the same subspace to yield the desired complete source presents a non-trivial task. Yet, given that a portion of the information is shared among different sources, it is feasible to establish transformation between them by identifying a common source. We subsequently cast the problem of identifying a common source as one of optimal transport objectives, which involves searching plans to move factors from view-specific sources to the common source.

Permutation learning Assume there is a common source $c_t \in \mathbb{R}^{d_c}$ shared across all view-specific sources z_t^v . While directly searching for the correspondence of common components can be infeasible, we propose to enforce the c_t^v be in the top- d_c channels of z_t^v via permutation learning. Formally, we can achieve this by multiplying the z_t^v with a doubly stochastic matrix $B^v \in \mathfrak{B}_{d_v}$ as follows,

$$\bar{z}_t^v = B^v \hat{z}_t^v, \quad c_t^v = \bar{z}_{1:d_c,t}^v. \quad (8)$$

After that, we can impose the permutations that generate embeddings whose top d_c entries are most correlated:

$$\max_{\{B^v\}} \mathbb{E}_{v \neq v'} \text{Tr} \left((B^v \hat{z}_t^v)_{1:d_c} (B^{v'} \hat{z}_t^{v'})_{1:d_c}^\top \right). \quad (9)$$

In essence, our goal is to ensure that all extracted instances of $\{c_t^v\}$ have entries closely resembling those of the identified common components. Notably, the procedure outlined above equates to regularizing these $\{c_t^v\}$ so that they are concentrated around their mean. To achieve this, we first estimate a mean center from the currently extracted common sources:

$$c_t^* = \arg \min_{c_t \in \mathbb{R}^{d_c}} \sum_v \|c_t^v - c_t\|^2. \quad (10)$$

In practice, we achieve the objective of Eq. (9) by updating the transport plans $\{B^v\}$ and minimizing transport cost from top- d_c view specific components to c_t^* in an alternating manner:

$$\mathcal{L}_m = \sum_{v=1}^2 \mathbb{E} \left[\|(B^v z_t^v)_{1:d_c} - c_t^*\|^2 \right] + \eta R(B^v), \quad (11)$$

where $R(B^v) = -\sum_{i,j} B_{i,j}^v \log(B_{i,j}^v)$, $\eta > 0$ is a constant. This criterion effectively results in learning that $c_t^1 = c_t^2$, which represents the ultimate solution for the merging of latent variables.

After this reformulation, with the center c_t^* fixed, we can search for the locally optimal $\{B^v\}$ separately. Crucially, each sub-problem now becomes a standard combinatorial assignment problem [Peyré and Cuturi, 2018], which involves the search for optimal transport plans that assign

common components from view-specific sources to the common source c_t^* . Ultimately, by iteratively applying the center mean estimation procedure from Eq. (10) and utilizing the Sinkhorn algorithm, we can achieve the minimizer of our final objective, as expressed in Eq. (11) (refer to Appendix B for additional details). We can consider the application of the transformation B^v as a process of smooth component sorting. When we can identify estimated latent sources up to a permutation transformation, we can reduce the doubly stochastic matrices B^v to permutation matrices, i.e., $\{P^v | P^v \in \{0,1\}^{d_v \times d_v}\}$. This resolution addresses the issue of non-corresponding components.

For merge operator m , we concatenate the c_t^* with all remaining private components:

$$\hat{z}_t = \begin{bmatrix} c_t^* \\ \bar{z}_{d_c+1:d_1,t}^1 \\ \bar{z}_{d_c+1:d_2,t}^2 \end{bmatrix} = m \left(\begin{bmatrix} \hat{z}_t^1 \\ \hat{z}_t^2 \end{bmatrix} \right). \quad (12)$$

Consequently, we can input the merged latent source into the contrastive learning and the inference of causal relations, as outlined in Sec 2.2, thereby completing the entire objective.

Theorem 2 (Minimizers of the multi-view objective maintains the channel correspondency). *Let $\mathcal{Z}^v \subseteq \mathbb{R}^{d_v}$, $\mathcal{Z} = \cup \mathcal{Z}^v$ and $\cap \mathcal{Z}^v \neq \emptyset$. If $B^v \in \mathfrak{B}_{d_v}$ be a doubly stochastic matrix, $r, f, \{B^v\}$ are the minimizers of contrastive objective for $M \rightarrow +\infty$, then, we have $h = r \circ g$ is an isometry, and $\{B^v\}$ can rearrange the components of each view source such that common components from each view source are aligned.*

3 Optimization

We use deep neural networks to implement $f(\cdot)$ and $r^v(\cdot)$. The process of learning latent variables z_t from multi-view data involves contrastive learning on estimated latent variables and the learning of permutations for view-specific variables. We jointly train view-specific reverse networks as well as a causal transition network. The permutation matrices $\{B^v\}$ are also alternatively optimized during this process.

Enhance noises distribution learning Contrastive learning is designed to minimize the distance between positive pairs, in other words, it brings \hat{z}_t and $f(\hat{z}_{H_t})$ closer together. To emphasize this property, we further employ an objective to minimize the residual as:

$$\mathcal{L}_\epsilon = \mathbb{E}[\delta(\hat{z}_t, f(\hat{z}_{H_t}))]. \quad (13)$$

In parallel, to enhance the mutual independence property of noise $\epsilon_{i,t}$, we follow the approach of [Yao *et al.*, 2021] and create a discriminator network $\mathcal{D}(\cdot)$ implemented by MLPs. This network is used for discriminating the $\{\hat{\epsilon}_{i,t}\}$ and randomly permuted versions $\{\hat{\epsilon}_{i,t}\}^{\text{perm}}$,

$$\mathcal{L}_{\mathcal{D}} = \mathbb{E}[\log \mathcal{D}(\{\hat{\epsilon}_{i,t}\}) - \log(1 - \mathcal{D}(\{\hat{\epsilon}_{i,t}\}))]. \quad (14)$$

Combining all these elements with weights, the objective is:

$$\mathcal{L} = \mathcal{L}_{\text{contr}} + \beta_1 \mathcal{L}_m + \beta_2 \mathcal{L}_\epsilon + \beta_3 \mathcal{L}_{\mathcal{D}}. \quad (15)$$

For stable training, we perform the optimization of $\mathcal{L}_{\text{contr}}$ and \mathcal{L}_m alternately.

4 Experiments

In this section, we present our experimental results on three multi-view scenarios to validate the superiority of MuLTI. More empirical results can be found in Appendix D.

4.1 Datasets

We use synthetic and real-world datasets for evaluating the latent process identification task. Different view-specific encoders are used in different datasets for extracting latent variables. In what follows, we briefly introduce the datasets.

Multi-view VAR is a synthetic dataset modified from [Yao *et al.*, 2021]. To generate the latent process, we first select transition matrices $\{A_\tau\}_{\tau=1}^L$ from a uniform distribution $U[-0.5, 0.5]$, and then sample initial states $\{z_t\}_{t=1}^L$ from a normal distribution to generate sequences $\{z_t\}_{t=1}^L$. To generate multi-view time series, we randomly select d_1 and d_2 dimensions of latent variables for each view. The nonlinear observations of each view are created by mixing latent variables with randomly parameterized MLPs $g^v(\cdot)$ following the previous work [Hyvärinen and Morioka, 2017].

Mass-spring system is a video dataset adopted from [Li *et al.*, 2020] specifically designed for a multi-view setting. A mass-spring system consists of 8 movable balls; the balls are either connected by springs or are not connected at all. As a result of random external forces, the system exhibits different dynamic characteristics depending on its current state and internal constraints. We create two views for this video dataset, as shown in Figure 4, in each of which only 5 of the 8 balls are observable. Consequently, each pair of views includes two videos, each with a duration of 80 frames. This dataset contains 5,000 pairs of video clips in total.

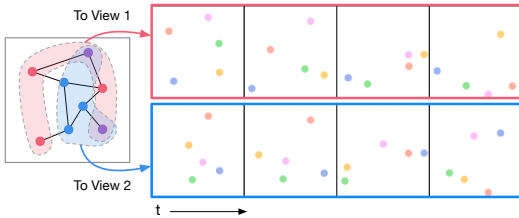


Figure 4: Illustration of multi-view Mass-spring system.

Multi-view UCI Daily and Sports Activities [Altun *et al.*, 2010] is a multivariate time series dataset comprising 9,120 sequences, capturing sensor data for 19 different human actions performed by 8 subjects. Each sample activity contains 125 time steps, each captured by nine sensors, yielding a total of 45 dimensions. We construct the multi-view setting following the [Li *et al.*, 2016]. The 27 dimensions located on the torso, right arm, and left arm are collectively regarded as view 1, while the remaining 18 dimensions on the left and right legs constitute view 2.

4.2 Evaluation Setup

To measure the identifiability of latent causal variables, we compute Mean Correlation Coefficient (MCC) on the validation datasets for revealing the indeterminacy up to permutation transformations, and R^2 for revealing the indeterminacy up to linear transformations. We assess the accuracy of

our causal relations estimations by comparing them with the actual data structure, quantified via the Structural Hamming Distance (SHD) on the validation datasets.

Baselines Four different methods for estimating latent variables: (1) BetaVAE [Higgins *et al.*, 2017] neither accounts for the temporal structure nor provides an identifiability guarantee; (2) SlowVAE [Klindt *et al.*, 2021], PCL [Hyvärinen and Morioka, 2017], and GCL [Hyvärinen *et al.*, 2019] identify independent sources from observations; (3) ShICA [Richard *et al.*, 2021] identifies the shared sources from multi-view observations; (4) CL-ICA [Zimmermann *et al.*, 2021] recovers the latent variables via contrastive learning; (5) LEAP [Yao *et al.*, 2021] utilizes temporally engaged sources and causal mechanism but only suitable single view data.

For multi-view time series adaptation of baseline methods – β -VAE, SlowVAE, PCL, CL-ICA, and LEAP – we concatenate the series into single-view format, aligning them by the feature dimension. In the GCL setting, we designate as positive pairs the views originating from the same source, and negative pairs those stemming from distinct sources.

Implementation details For the Multi-view VAR dataset, we use architectures composed of MLPs and Leaky ReLU units. Ground-truth latent variable dimension d is set to 10, the noise distribution is set to Laplacian(0, 0.05). We set the batch size to 2400, employ the Adam optimizer with a learning rate of 0.001, and utilize $\beta_1 = 0.01, \beta_2 = 0.01, \beta_3 = 1e - 5$. To verify the influence of the overlapping ratio of views, we select $d_c \in \{10, 4, 2, 0\}$ for evaluation. Here, $d_c = 0$ and $d_c = 10$ indicate situations where the latent variables for generating views are fully overlapped and have no overlaps, respectively. To ensure a fair comparison, all baseline methods utilize similar encoders, and the time-lag L of the causal transition module is set to equal the ground truth.

For the Mass-spring system, we create view-specific encoders following [Li *et al.*, 2020], which has similar architectures to the unsupervised keypoints discovery perception module. We set the time lag $L = 2$ for the causal transition module as the approximated process corresponds to a mass-spring system, which is a dynamic system of second order. The dimension of estimated latent variables is set to be the same as ground-truth, *i.e.*, 8 coordinates (x, y) account for $d = 16$. In practice, we first pre-train two pairs of keypoint encoder-decoder in each view. Then, the pre-trained encoders are taken as $r^v(\cdot)$ corresponding to each view.

For the Multi-view UCI dataset, we construct two separate encoders with MLPs for two views. The latent dimensions of view 1 and view 2 are set to $d_1 = 12$ and $d_2 = 9$ respectively, the shared latent dimension is set to $d_c = 3$, and the complete latent dimension accounts for $d = 18$. The time lag of the causal transition module is set to $L = 1$. We initially train the MuLTI on the complete dataset, following which we extract the latent variables for downstream tasks.

4.3 Main Results

MuLTI achieves the best identifiability We report both R^2 and MCC in Table 1 for revealing the identifiability of each method. As shown in the results, MuLTI achieves the best identifiability across most settings, particularly over the

Table 1: Identifiability results on the VAR process ($d = 10, L = 2$). Mean+standard deviation over 5 random seeds.

Methods	R^2 (%)				MCC			
	$d_c = d$	$d_c = 4$	$d_c = 2$	$d_c = 0$	$d_c = d$	$d_c = 4$	$d_c = 2$	$d_c = 0$
β -VAE	40.03 \pm 5.31	41.43 \pm 4.22	40.67 \pm 3.44	38.36 \pm 2.71	29.37 \pm 8.20	38.31 \pm 6.31	31.92 \pm 5.61	41.88 \pm 4.62
SlowVAE	60.32 \pm 5.56	63.21 \pm 5.51	62.12 \pm 6.13	61.23 \pm 3.17	50.32 \pm 3.49	51.24 \pm 4.71	52.55 \pm 2.39	54.21 \pm 3.07
PCL	69.78 \pm 3.20	80.24 \pm 3.32	75.71 \pm 2.71	74.56 \pm 2.90	52.64 \pm 2.33	54.63 \pm 2.12	53.42 \pm 1.91	55.61 \pm 2.62
GCL	73.45 \pm 4.34	82.41 \pm 3.12	77.65 \pm 2.52	73.21 \pm 3.31	53.55 \pm 1.71	57.32 \pm 2.41	52.42 \pm 1.70	55.23 \pm 2.31
ShICA	41.08 \pm 5.76	39.65 \pm 4.51	37.61 \pm 4.32	38.43 \pm 3.12	28.71 \pm 5.21	37.21 \pm 5.13	29.31 \pm 4.97	31.47 \pm 3.61
CL-ICA	21.48 \pm 6.71	29.37 \pm 4.32	24.27 \pm 3.33	23.89 \pm 2.71	26.79 \pm 5.51	33.35 \pm 4.51	29.39 \pm 5.11	23.68 \pm 4.90
LEAP	99.59 \pm 0.05	99.67 \pm 0.09	99.48 \pm 0.07	99.74 \pm 0.06	57.56 \pm 2.44	62.48 \pm 2.12	65.44 \pm 1.61	67.75 \pm 1.32
MuLTI	99.46 \pm 0.09	99.72 \pm 0.05	99.68 \pm 0.07	99.45 \pm 0.08	99.80 \pm 0.12	99.27 \pm 0.43	99.39 \pm 0.09	99.43 \pm 0.04

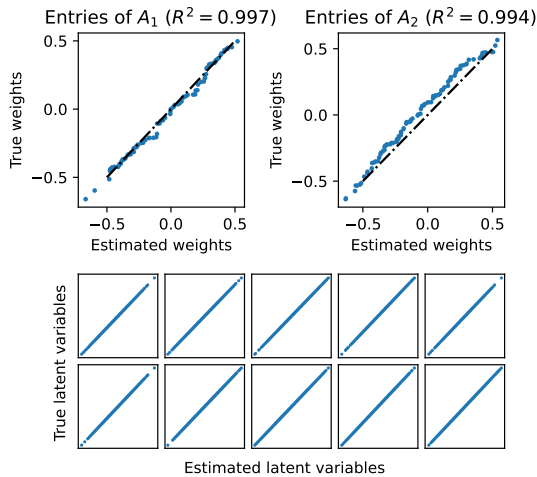


Figure 5: Results for latent VAR process ($d = 10, d_c = 2$) identification. Scatters are paired estimations and ground-truth.

MCC metrics, where MuLTI outperforms all rivals by a notable margin. The results indicate that, without modeling the causal transition in the conditional distribution, the independence conditions of methods such as β -VAE, SlowVAE, ShICA, CL-ICA, PCL, and GCL fail to recover the latent variables, even up to linear transformations. LEAP successfully identifies the latent process up to linear transformations using causal transition constraints. Yet, it struggles to recover the process up to permutation transformation for observations from distinct views, despite conditions suitable for permutation identifiability.

MuLTI successfully identifies the latent process We show that MuLTI successfully identifies the latent process on both the Multi-view VAR dataset and the Mass-spring system. Figure 5 demonstrates the performance of our MuLTI in estimating the latent process where $d = 10, d_c = 2$. The results suggest that our model nearly perfects the learning of the VAR transition matrices, with the identified latent variables closely resembling the true variables, thus implying a comprehensive identification of the latent process.

The objective of the Mass-spring system task is to estimate latent variables, representing the coordinates of each ball, and transition matrices that elucidate their connections.

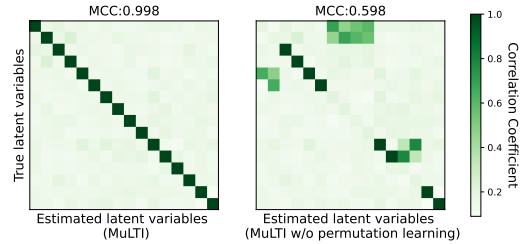


Figure 6: Correlation matrix of recovered latent variables vs. ground-truth latent variables of Mass-spring system.

As displayed in the left panel of Figure 6, the estimated latent variables precisely match the ground-truth, and the recovered transition matrices correspond to the ground-truth ball connections, as indicated by an SHD = 0.

MuLTI improves downstream task Given that causal variables are often not readily available, directly assessing their identification and relationships in real-world data proves challenging. However, under most conditions, identifying the latent process from observations can simplify downstream tasks (*e.g.*, classification and clustering) or directly aid in the extraction of meaningful features. Therefore, we employ a real-world multi-view time series dataset to demonstrate the effectiveness of latent process identification. We employ multivariate time series classifiers - specifically, reservoir computing [Bianchi *et al.*, 2021]. This approach encodes the multivariate time series data into a vectorial representation in an unsupervised manner, allowing us to evaluate learned latent variables $\{\hat{z}_t\}_{t=1}^T$ in the downstream task.

To demonstrate the efficacy of the learned latent representations, we independently train both the baseline methods and MuLTI on the entire dataset, subsequently extracting 18-dimensional features to form a new dataset. Then, we train and evaluate the RC classifier on the new datasets extracted by each method. The results are shown in Table 2. We report classification accuracy with varying training set sizes, *i.e.*, we randomly select $N_{tr} \in \{10, 20, 30, 40, 50\}$ samples per class for training, using the remaining samples for testing. Compared to the baseline methods, the pre-trained features from MuLTI enhance the downstream performance of the RC classifier, particularly for small training set classification tasks.

Table 2: Classification accuracy on Multi-view UCI dataset. N_{tr} is the number of training samples randomly chosen from each class.

N_{tr}	raw data	+ β -VAE	+LEAP	+ShICA	+MuLTI
10	74.21 \pm 0.26	72.53 \pm 1.13	73.57 \pm 1.90	73.17 \pm 0.77	85.59 \pm 0.05
20	90.00 \pm 0.38	85.82 \pm 0.53	86.10 \pm 0.86	86.59 \pm 0.51	92.14 \pm 0.38
30	92.92 \pm 0.74	89.37 \pm 1.54	88.90 \pm 0.69	91.29 \pm 0.31	94.18 \pm 0.14
40	94.95 \pm 0.16	91.16 \pm 0.49	91.79 \pm 0.07	94.01 \pm 0.55	96.15 \pm 0.81
50	94.92 \pm 0.28	92.53 \pm 0.04	93.00 \pm 0.03	94.78 \pm 0.04	96.82 \pm 0.30

Table 3: Ablation results on VAR dataset ($d = 10, d_c = 4, L = 2$).

MuLTI	R^2 (%)	MCC
w/o Causal transition	44.67 \pm 2.31	33.47 \pm 7.60
w/o Permutation learning	99.32 \pm 0.07	77.45 \pm 0.47
w/o Residuals minimization	99.48 \pm 0.04	82.32 \pm 2.63
w/o Noise discriminator	99.23 \pm 0.05	98.32 \pm 0.27

4.4 Ablation Studies

Module ablations To verify the effectiveness of each module within MuLTI, we conduct ablation studies by individually removing each module. The results tested on the Multi-view VAR dataset are shown in Table 3. When the causal transition module is removed, positive pairs are formed from temporally adjacent states, *i.e.*, $(\hat{z}_t, \hat{z}_{t+1})$. In the setting of removing permutation learning, the view-specific variables are simply concatenated along the feature dimension and mapped with a linear layer to match the dimension of the transition function. Results indicate the crucial role of the causal transition function in identifying the spatial-temporal dependent latent process. As shown, permutation learning also greatly contributes to the identifiability under this multi-view setting. Furthermore, Figure 6 from the Mass-spring system experiment reveals that, without permutation learning, only partial identification of the latent variables is possible.

Effect of noise and distance metrics To evaluate the effect of noise distribution type and distance metric $\delta(\cdot, \cdot)$, we conduct experiments under different combinations. The results shown in Table 4 indicate that the Laplacian noise condition accompanied with ℓ_1 norm is key to identifying the ground-truth latent processes up to permutation equivalence. Nevertheless, in most conditions, we can still identify the latent process up to linear equivalence.

5 Related Works

Multi-view representation learning Many realistic conditions involve data from multiple channels and domains; these data must be analyzed together in order to obtain a reliable estimation of latent relations, *e.g.* neurophysiology and behavior time series data [Urai *et al.*, 2022]. Typical methods of learning share representations from multi-view data include Canonical Correlation Analysis (CCA) [Hotelling, 1992] and its variants [Akaho, 2006; Andrew *et al.*, 2013; Lai and Fyfe, 2000; Wang *et al.*, 2015; Zhao *et al.*, 2017], but most of these methods only consider learning the common source of each view. More recently, some improve-

Table 4: Identifiability with different noise prior & metric. Note that the *Identity* indicates the untrained model, and *Supervised* indicates the model trained with MSE between ground-truth and estimated latent variables. Mean+standard deviation over 5 random seeds.

Noise type	$\delta(\cdot, \cdot)$	R^2 (%)	MCC
Identity	/	66.12 \pm 2.77	43.91 \pm 2.56
Supervised	/	99.78 \pm 0.07	99.92 \pm 0.02
Normal ($\sigma = 0.1$)	ℓ_2	99.72 \pm 0.03	67.21 \pm 1.41
Laplace ($\lambda = 0.1$)	ℓ_2	99.71 \pm 0.02	66.74 \pm 0.21
Normal ($\sigma = 0.1$)	ℓ_1	99.69 \pm 0.04	70.52 \pm 0.27
Laplace ($\lambda = 0.1$)	ℓ_1	99.74 \pm 0.02	99.31 \pm 0.07
Laplace ($\lambda = 0.05$)	ℓ_1	99.77 \pm 0.03	99.81 \pm 0.02

ments are done in dividing the sources into common and private components [Lyu *et al.*, 2021; Huang *et al.*, 2018; Hwang *et al.*, 2020; Luo *et al.*, 2022]. However, it is not the case when there are relations (causal influences) between source components, due to most of them relying on independent source assumptions [Gresele *et al.*, 2019]. In contrast, our work seeks to recover latent variables when there are causal relations between them.

Identifiability Identifiability means the estimated latent variables are exactly equivalent to the underlying ones or at least up to simple transformation. Traditional independent component analysis (ICA) [Belouchrani *et al.*, 1997] assumes sources are linear mixed, but such linearity relation may not hold in many applications. To overcome this limitation, the non-linear ICA (nICA) [Hyvärinen and Pajunen, 1999] has attracted great attention. A variety of practical methods [Hyvärinen and Morioka, 2017; Hyvärinen *et al.*, 2019; Khemakhem *et al.*, 2020; Sorrenson *et al.*, 2020] have been proposed to achieve identifiability through discriminating data structures, such as manually constructing positive and negative pairs and training models to produce features to distinguish whether input data are distorted, such as temporal structure [Hyvärinen and Morioka, 2016] and randomized distorted data pairs [Hyvärinen *et al.*, 2019]. More recently, Gresele *et al.* adopt similar practices into multi-view data, but still limited in source independent assumptions. Yao *et al.* make attempts on dependent sources but their method can only handle single-view data. In this work, we explore a general case that identifies dependent processes from multi-view temporal data.

6 Conclusion

In this work, we make the first attempt toward a general setting of the multi-view latent process identification problem and propose a novel MuLTI framework based on contrastive learning. The key idea is to identify the latent variables and dependent structure through the construction of conditional distribution and aggregating variables across views. Empirical results suggest that our methods can successfully identify the spatial-temporal dependent latent process from multi-view time series observations. We hope our work can raise more attention to the importance of identifying and aggregating latent factors in understanding multi-view data.

7 Acknowledgments

This work is supported by the National Key R&D Program of China (2020YFB1313501), National Natural Science Foundation of China (T2293723, 61972347), Zhejiang Provincial Natural Science Foundation (LR19F020005), the Key R&D program of Zhejiang Province (2021C03003, 2022C01119, 2022C01022), the Fundamental Research Funds for the Central Universities (No. 226-2022-00051). JZ also want to thank the support by the NSFC Grants (No. 62206247) and the Fundamental Research Funds for the Central Universities.

References

- [Akaho, 2006] Shotaro Akaho. A kernel method for canonical correlation analysis. *arXiv preprint cs/0609071*, 2006.
- [Altun *et al.*, 2010] Kerem Altun, Billur Barshan, and Orkun Tunçel. Comparative study on classifying human activities with miniature inertial and magnetic sensors. *Pattern Recognition*, 2010.
- [Andrew *et al.*, 2013] Galen Andrew, Raman Arora, Jeff Bilmes, and Karen Livescu. Deep canonical correlation analysis. In *International Conference on Machine Learning*, pages 1247–1255. PMLR, 2013.
- [Belouchrani *et al.*, 1997] Adel Belouchrani, Karim Abed-Meraim, J-F Cardoso, and Eric Moulines. A blind source separation technique using second-order statistics. *IEEE Transactions on signal processing*, 1997.
- [Bianchi *et al.*, 2021] Filippo Maria Bianchi, Simone Scardapane, Sigurd Løkse, and Robert Jenssen. Reservoir Computing Approaches for Representation and Classification of Multivariate Time Series. *IEEE Transactions on Neural Networks and Learning Systems*, 2021.
- [Chickering, 2002] David Maxwell Chickering. Optimal structure identification with greedy search. *Journal of machine learning research*, 2002.
- [Ding *et al.*, 2006] Mingzhou Ding, Yonghong Chen, and Steven L Bressler. Granger causality: Basic theory and application to neuroscience. *Handbook of time series analysis: recent theoretical developments and applications*, 2006.
- [Gresele *et al.*, 2019] Luigi Gresele, Paul K. Rubenstein, Arash Mehrjou, Francesco Locatello, and Bernhard Schölkopf. The incomplete rosetta stone problem: Identifiability results for multi-view nonlinear ICA. In *Proc. of UAI*, 2019.
- [He *et al.*, 2021] Guoliang He, Han Wang, Shenxiang Liu, and Bo Zhang. CSMVC: A Multiview Method for Multivariate Time-Series Clustering. *IEEE Transactions on Cybernetics*, 2021.
- [Higgins *et al.*, 2017] Irina Higgins, Loïc Matthey, Arka Pal, Christopher Burgess, Xavier Glorot, Matthew Botvinick, Shakir Mohamed, and Alexander Lerchner. beta-vae: Learning basic visual concepts with a constrained variational framework. In *Proc. of ICLR*, 2017.
- [Hotelling, 1992] Harold Hotelling. Relations Between Two Sets of Variates. In *Breakthroughs in Statistics*. Springer New York, 1992.
- [Hoyer *et al.*, 2008] Patrik O. Hoyer, Dominik Janzing, Joris M. Mooij, Jonas Peters, and Bernhard Schölkopf. Nonlinear causal discovery with additive noise models. In *Proc. of NeurIPS*, 2008.
- [Huang *et al.*, 2018] Xun Huang, Ming-Yu Liu, Serge Belongie, and Jan Kautz. Multimodal unsupervised image-to-image translation. In *Proc. of ECCV*, 2018.
- [Hwang *et al.*, 2020] HyeongJoo Hwang, Geon-Hyeong Kim, Seunghoon Hong, and Kee-Eung Kim. Variational interaction maximization for cross-domain disentanglement. In *Proc. of NeurIPS*, 2020.
- [Hyvärinen and Morioka, 2016] Aapo Hyvärinen and Hiroshi Morioka. Unsupervised feature extraction by time-contrastive learning and nonlinear ICA. In *Proc. of NeurIPS*, 2016.
- [Hyvärinen and Morioka, 2017] Aapo Hyvärinen and Hiroshi Morioka. Nonlinear ICA of temporally dependent stationary sources. In *Proc. of AISTATS*, 2017.
- [Hyvärinen and Pajunen, 1999] Aapo Hyvärinen and Petteri Pajunen. Nonlinear independent component analysis: Existence and uniqueness results. *Neural Networks*, 1999.
- [Hyvärinen *et al.*, 2019] Aapo Hyvärinen, Hiroaki Sasaki, and Richard E. Turner. Nonlinear ICA using auxiliary variables and generalized contrastive learning. In *Proc. of AISTATS*, 2019.
- [Khemakhem *et al.*, 2020] Ilyes Khemakhem, Diederik P. Kingma, Ricardo Pio Monti, and Aapo Hyvärinen. Variational autoencoders and nonlinear ICA: A unifying framework. In *Proc. of AISTATS*, 2020.
- [Klindt *et al.*, 2021] David A. Klindt, Lukas Schott, Yash Sharma, Ivan Ustyuzhaninov, Wieland Brendel, Matthias Bethge, and Dylan M. Paiton. Towards nonlinear disentanglement in natural data with temporal sparse coding. In *Proc. of ICLR*, 2021.
- [Lai and Fyfe, 2000] P. L. Lai and C. Fyfe. Kernel and nonlinear canonical correlation analysis. *International Journal of Neural Systems*, 2000.
- [Li *et al.*, 2016] Sheng Li, Yaliang Li, and Yun Fu. Multi-view time series classification: A discriminative bilinear projection approach. In *Proc. of CIKM*, 2016.
- [Li *et al.*, 2020] Yunzhu Li, Antonio Torralba, Anima Anandkumar, Dieter Fox, and Animesh Garg. Causal discovery in physical systems from videos. In *Proc. of NeurIPS*, 2020.
- [Luo *et al.*, 2022] Dixin Luo, Hongteng Xu, and Lawrence Carin. Differentiable Hierarchical Optimal Transport for Robust Multi-View Learning. *IEEE Transactions on Pattern Analysis and Machine Intelligence*, 2022.
- [Lyu *et al.*, 2021] Qi Lyu, Xiao Fu, Weiran Wang, and Songtao Lu. Understanding latent correlation-based multiview learning and self-supervision: An identifiability perspective. In *Proc. of ICLR*, 2021.

- [Pearl, 2000] Judea Pearl. *Causality: Models, Reasoning, and Inference*. Cambridge University Press, Cambridge, U.K. ; New York, 2000.
- [Peyré and Cuturi, 2018] Gabriel Peyré and Marco Cuturi. *Computational Optimal Transport*, 2018.
- [Richard *et al.*, 2021] Hugo Richard, Pierre Ablin, Bertrand Thirion, Alexandre Gramfort, and Aapo Hyvarinen. Shared Independent Component Analysis for Multi-Subject Neuroimaging. In *Proc. of NeurIPS*, 2021.
- [Sorenson *et al.*, 2020] Peter Sorenson, Carsten Rother, and Ullrich Köthe. Disentanglement by nonlinear ICA with general incompressible-flow networks (GIN). In *Proc. of ICLR*, 2020.
- [Spirtes *et al.*, 2000] Peter Spirtes, Clark N. Glymour, Richard Scheines, and David Heckerman. *Causation, Prediction, and Search*. MIT Press, 2000.
- [Tsamardinos *et al.*, 2006] Ioannis Tsamardinos, Laura E. Brown, and Constantin F. Aliferis. The max-min hill-climbing Bayesian network structure learning algorithm. *Machine Learning*, 2006.
- [Urai *et al.*, 2022] Anne E. Urai, Brent Doiron, Andrew M. Leifer, and Anne K. Churchland. Large-scale neural recordings call for new insights to link brain and behavior. *Nature Neuroscience*, 2022.
- [van den Oord *et al.*, 2018] Aaron van den Oord, Yazhe Li, and Oriol Vinyals. Representation Learning with Contrastive Predictive Coding, 2018.
- [Wang *et al.*, 2015] Weiran Wang, Raman Arora, Karen Livescu, and Jeff A. Bilmes. On deep multi-view representation learning. In *Proc. of ICML*, 2015.
- [Wang *et al.*, 2020] Heyuan Wang, Tengjiao Wang, and Yi Li. Incorporating expert-based investment opinion signals in stock prediction: A deep learning framework. In *Proc. of AAAI*, 2020.
- [Yao *et al.*, 2021] Weiran Yao, Yuewen Sun, Alex Ho, Changyin Sun, and Kun Zhang. Learning Temporally Causal Latent Processes from General Temporal Data. In *Proc. of ICLR*, 2021.
- [Zhang, 2008] Jiji Zhang. On the completeness of orientation rules for causal discovery in the presence of latent confounders and selection bias. *Artificial Intelligence*, 2008.
- [Zhao *et al.*, 2017] Handong Zhao, Zhengming Ding, and Yun Fu. Multi-view clustering via deep matrix factorization. In *Proc. of AAAI*, 2017.
- [Zheng *et al.*, 2018] Xun Zheng, Bryon Aragam, Pradeep Ravikumar, and Eric P. Xing. Dags with NO TEARS: continuous optimization for structure learning. In *Proc. of NeurIPS*, 2018.
- [Zimmermann *et al.*, 2021] Roland S. Zimmermann, Yash Sharma, Steffen Schneider, Matthias Bethge, and Wieland Brendel. Contrastive learning inverts the data generating process. In *Proc. of ICML*, 2021.

A Notations and Terminology

Table A.1: List of notations.

Index	
i, j	Variable element (vector/matrix element) index
t	Time step
τ	Time delay step
v	View index
H_t	A set of indices represent the previous time steps back from the t -step
Variable	
\mathbf{x}_t^v	Observations of v -th view
\mathbf{z}_t	Ground-truth latent source variable at t -step
\mathbf{z}_t^v	Ground-truth latent source variable of v -th view
$\epsilon_{t,i}$	Mutually independent exogenous noise variable in generating $\mathbf{z}_{t,i}$
$\hat{\mathbf{z}}_t$	Reconstructed factors by $r(\cdot)$
$\tilde{\mathbf{z}}_t$	Positive pair of \mathbf{z}_t
$\mathbf{Pa}(\cdot)$	Set of direct cause nodes/parents of variable $\mathbf{z}_{t,i}$
\mathbf{A}_τ	Transition matrix with τ steps delay
\mathfrak{B}_d	d -dimensions Birkhoff polytope
\mathbf{B}^v	$\mathbf{B}^v \in \mathfrak{B}_{d_v}$ is the doubly stochastic matrix with d_v -dimensions
μ	Temperature constant for contrastive learning
η	Doubly stochastic matrix entropy penalty scale factor
Function and Hyper-parameter	
g	Potential invertible function which control the v_i generating
r	Function which encodes data to latent factors
h	$h = r \circ g : \mathcal{Z} \mapsto \mathcal{Z}$ the transformation between ground-truth and estimated factors
f	Causal transition function which encodes time-delayed causal relations between factors

B Permutation Learning for the Merge Operation

In this section, we briefly introduce the optimization of permutation learning. As indeterminacy exists in encoded view-specific variables, permutation learning is a preliminary step towards merging operations by searching for the order correspondence between components across views.

Recall that we adopt an alternative optimization strategy to optimize the overall objective. Specifically, to perform permutation learning, we freeze other modules of the model to optimize the permutation matrices and the resultant objective is as follows:

$$\min_{\mathbf{B}^v} \mathbb{E} [\|(\mathbf{B}^v \mathbf{z}_t^v)_{1:d_c} - \mathbf{c}_t^*\|^2] + \eta R(\mathbf{B}^v),$$

where $R(\mathbf{B}^v) = -\sum_{i,j} B_{i,j} \log B_{i,j}$, and \mathbf{c}_t^* can be regarded as a mean variable of all shared components. Technically, we keep a set of trainable matrices $\{\mathbf{B}^v\}$ that correspond to the dimension permutations for each view-specific encoder. At each permutation matrix optimization step,

MULTI searches for top- d_c most relevant components between view-specific latent variables. Note that if the component is correctly ordered, each shared components are able to match each other, which leads to a low variance in this dimension. Hence, optimizing Eq. (9) induces a set of proper permutation matrices for merging the latent factors from different views.

The approximate permutation matrices $\{\mathbf{B}^v\}$ should follow some constraints in order to prevent the degradation of permutation learning, namely, to keep every \mathbf{B}^v within the Birkhoff Polytope at the whole procedure. Let \mathcal{B}_d denote the d -Birkhoff polytope, i.e., the set of doubly stochastic matrices of dimension d , and \mathcal{P}_d denote the set of permutation matrices of dimension d ,

$$\mathcal{B}_d = \{\mathbf{B} \in [0, 1]^{d \times d}, \mathbf{B}\mathbf{1}_d = \mathbf{1}_d, \mathbf{B}^\top \mathbf{1}_d = \mathbf{1}_d\},$$

$$\mathcal{P}_d = \{\mathbf{B} \in \{0, 1\}^{d \times d}, \mathbf{B}\mathbf{1}_d = \mathbf{1}_d, \mathbf{B}^\top \mathbf{1}_d = \mathbf{1}_d\},$$

where \mathcal{P}_d indicates rigorous permutation, and \mathcal{B}_d indicates the relaxed version of the former. While our ultimate goal is to obtain a binary permutation matrix in \mathcal{P}_d , the objective can be hard to be resolved due to the discrete constraints. In practice, we search for a relaxed optimizer in \mathcal{B}_d to optimize Eq.(15) and finally binarize the obtained matrix to obtain the desired solution.

We decompose the optimization procedure into two steps. First, the standard stochastic gradient algorithm is applied to optimize Eq.(15), where \mathbf{B}^v s are searched in the \mathbb{R}^n space without considering the constraints. Next, denote the obtained matrix by \mathbf{M} , we introduce the Sinkhorn-Knopp method to transform it to a doubly stochastic matrix in \mathcal{B}_d . Let $S(\cdot)$ denote the Sinkhorn operator. The updating rule of the Sinkhorn-Knopp algorithm is as follows,

$$S^0(\mathbf{M}) = \exp(\mathbf{M}),$$

$$S^l(\mathbf{M}) = \mathcal{T}_{\text{col}}(\mathcal{T}_{\text{row}}(S^{l-1}(\mathbf{M}))),$$

$$S(\mathbf{M}) = \lim_{l \rightarrow \infty} S^l(\mathbf{M}),$$

where $\mathcal{T}_{\text{row}}(\mathbf{M}) = \mathbf{M} \oslash (\mathbf{M}\mathbf{1}_d\mathbf{1}_d^\top)$, and $\mathcal{T}_{\text{col}}(\mathbf{M}) = \mathbf{M} \oslash (\mathbf{1}_d\mathbf{1}_d^\top \mathbf{M})$ as row and column-wise normalization operators of matrix \mathbf{M} , with \oslash denoting the element-wise division and $\mathbf{1}_d$ a d dimensions vectors of ones. This operator has been proven that $S(\mathbf{M})$ must belong to the Birkhoff polytope \mathcal{B}_d [Kuhn, 1955]. In practice, we iterate up to 100 times to obtain an approximate doubly stochastic matrix. This number of iterations is usually around 20 \sim 100 to reach a satisfactory approximation. The whole Sinkhorn procedure is similar to the projected gradient descent algorithm.

At each permutation matrices freezing step, i.e., training the other modules of the model with permutation matrices fixed, we binarize $\{\mathbf{B}^v\}$ to obtain the closest true permutation matrix. Specifically, we fetch a rigorous permutation from a \mathbf{B}^v by solving:

$$\mathbf{P}^v = \arg \max_{\mathbf{P} \in \mathcal{P}_{d_v}} \langle \mathbf{P}, \mathbf{B}^v \rangle_F. \quad (16)$$

Then, we apply $\{\mathbf{P}^v\}$ to each view-specific variable for obtaining the top- d_c dimensions of each variable as common components across views.

The core of permutation learning is to implement trainable permutation matrices that “sort” the dimensions of each view-specific variable and assure common components in the same order. So we can select top- d_c dimensions of each view-specific variable and obtain the common variable \mathbf{c}_t^* .

C Proofs

C.1 Assumptions

Data-generating Process Let $\mathcal{Z} \in \mathbb{R}^d$ be the original source space and $\{\mathcal{X}^v \in \mathbb{R}^{D_v}\}$ be a set of observational spaces. We assume that the marginal distribution $p(\mathbf{z}_t)$ where $\mathbf{z}_t \in \mathcal{Z}$ is uniform:

$$p(\mathbf{z}_t) = \frac{1}{|\mathcal{Z}|}. \quad (17)$$

And there are series of injective functions $g^v : \mathcal{Z}^v \mapsto \mathcal{X}^v$ where $\cup \mathcal{Z}^v = \mathcal{Z}$.

Combining the causal transition function f which generates the latent variable \mathbf{z}_t from the previous states

$$\mathbf{z}_t = f(\mathbf{Pa}(\mathbf{z}_t), \epsilon_t), \quad (18)$$

where ϵ_t is a mutual independent noise with zero mean. From the parameters estimation perspective, ϵ_t is independent of the parameters of f . Hence, we denote $\tilde{\mathbf{z}}_t$ as a recursion of noiseless causal transition $\tilde{\mathbf{z}}_t = f(\mathbf{Pa}(\mathbf{z}_t))$ which is also assumed to be uniformly distributed with $p(\tilde{\mathbf{z}}_t) = |\mathcal{Z}|^{-1}$. Note, the $\tilde{\mathbf{z}}_t$ and \mathbf{z}_t differ by the noise term ϵ_t , therefore we can model the conditional distribution as:

$$p(\tilde{\mathbf{z}}_t | \mathbf{z}_t) = C_p^{-1} e^{-\delta(\mathbf{z}_t, \tilde{\mathbf{z}}_t)} \\ \text{with } C_p(\mathbf{z}_t) := \int e^{-\delta(\mathbf{z}_t, \tilde{\mathbf{z}}_t)} d\tilde{\mathbf{z}}_t, \quad (19)$$

where $\delta(\cdot, \cdot)$ is a semi-metric.

Model Let $r : \{\mathcal{X}^v\} \mapsto \mathcal{Z}^v$, where reverse function r is an abbreviation for a set of function r^v along with the merge operator. The reverse function encodes the observational data from different views into a unified representation \mathbf{z}_t . We use $h = r \circ g$ to represent the mapping between original space \mathcal{Z} and the estimated version. The modeled conditional distribution is expressed with h as $q_h(\tilde{\mathbf{z}}_t | \mathbf{z}_t)$ and

$$q_h(\tilde{\mathbf{z}}_t | \mathbf{z}_t) = C_h^{-1}(\mathbf{z}_t) e^{-\delta(h(\tilde{\mathbf{z}}_t), h(\mathbf{z}_t)) / \mu} \\ \text{with } C_h(\mathbf{z}_t) := \int e^{-\delta(h(\mathbf{z}_t), h(\tilde{\mathbf{z}}_t)) / \mu} d\tilde{\mathbf{z}}_t, \quad (20)$$

where $C_q(\mathbf{z}_t)$ is the partition function and $\mu > 0$ is a scale constant.

For modeling $\tilde{\mathbf{z}}_t$ with the causal transition function, we introduce the noiseless parametric causal transition:

$$\tilde{\mathbf{z}}_t = f(z_{H_t}) = \sum_{\tau=1}^L \mathbf{A}_\tau z_{t-\tau}, \quad (21)$$

C.2 Proof of Theorem 1

First, we introduce the following lemma extended from [Zimmermann *et al.*, 2021] to show the consistency of the connection between the cross-entropy and the contrastive loss.

Lemma 1 ($\mathcal{L}_{\text{contr}}$ converges to the cross-entropy between latent distribution). *If the ground-truth marginal distribution p is uniform, then for fixed $\mu > 0$, as the number of negative samples $M \rightarrow +\infty$, the (normalized) contrastive loss converges to*

$$\lim_{M \rightarrow +\infty} \mathcal{L}_{\text{contr}}(r; \mu, M) - \log M + \log |\mathcal{Z}| = \mathbb{E}_{\mathbf{z}_t \sim p(\mathbf{z}_t)} [H(p(\cdot | \mathbf{z}_t), q_h(\cdot | \mathbf{z}_t))], \quad (22)$$

where H is the cross-entropy between the ground-truth conditional distribution p over positive pairs and a conditional distribution q_h parameterized by the model r , and $C_h(\mathbf{z}_t) \in \mathbb{R}^+$ is the partition function of q_h :

$$q_h(\tilde{\mathbf{z}}_t | \mathbf{z}_t) = C_h(\mathbf{z}_t)^{-1} e^{-\delta(h(\tilde{\mathbf{z}}_t), h(\mathbf{z}_t)) / \mu} \\ \text{with } C_h(\mathbf{z}_t) := \int e^{-\delta(h(\tilde{\mathbf{z}}_t), h(\mathbf{z}_t)) / \mu}. \quad (23)$$

Proof. The cross-entropy between the conditional distribution p and q_h is given by

$$\mathbb{E}_{\mathbf{z}_t \sim p(\mathbf{z}_t)} [H(p(\cdot | \mathbf{z}_t), q_h(\cdot | \mathbf{z}_t))] \quad (24)$$

$$= \mathbb{E}_{\mathbf{z}_t \sim p(\mathbf{z}_t)} [\mathbb{E}_{\tilde{\mathbf{z}}_t \sim p(\tilde{\mathbf{z}}_t | \mathbf{z}_t)} [-\log q_h(\tilde{\mathbf{z}}_t | \mathbf{z}_t)]] \quad (25)$$

$$= \mathbb{E}_{\tilde{\mathbf{z}}_t, \mathbf{z}_t \sim p(\tilde{\mathbf{z}}_t, \mathbf{z}_t)} \left[\frac{1}{\mu} \delta(h(\tilde{\mathbf{z}}_t), h(\mathbf{z}_t)) + \log C_h(\mathbf{z}_t) \right] \quad (26)$$

$$= \mathbb{E}_{\mathbf{z}_t \sim p(\mathbf{z}_t)} \left[\frac{1}{\mu} \mathbb{E}_{\tilde{\mathbf{z}}_t \sim p(\tilde{\mathbf{z}}_t | \mathbf{z}_t)} [\delta(h(\tilde{\mathbf{z}}_t), h(\mathbf{z}_t))] + \log C_h(\mathbf{z}_t) \right], \quad (27)$$

which can be written as

$$\frac{1}{\mu} \mathbb{E}_{\substack{\mathbf{z}_t \sim p(\mathbf{z}_t) \\ \tilde{\mathbf{z}}_t \sim p(\tilde{\mathbf{z}}_t | \mathbf{z}_t)}} [\delta(h(\tilde{\mathbf{z}}_t), h(\mathbf{z}_t))] + \mathbb{E}_{\substack{\mathbf{z}_t \sim p(\mathbf{z}_t) \\ \tilde{\mathbf{z}}_t \sim p(\tilde{\mathbf{z}}_t | \mathbf{z}_t)}} [\log C_h(\mathbf{z}_t)]. \quad (28)$$

Inserting the definition of C_h gives

$$= \frac{1}{\mu} \mathbb{E}_{\substack{\mathbf{z}_t \sim p(\mathbf{z}_t) \\ \tilde{\mathbf{z}}_t \sim p(\tilde{\mathbf{z}}_t | \mathbf{z}_t)}} [\delta(h(\tilde{\mathbf{z}}_t), h(\mathbf{z}_t))] \quad (29)$$

$$+ \mathbb{E}_{\mathbf{z}_t \sim p(\mathbf{z}_t)} \left[\log \left(\int_{\mathcal{Z}} e^{-\delta(h(\tilde{\mathbf{z}}_t), h(\mathbf{z}_t)) / \mu} d\tilde{\mathbf{z}}_t \right) \right]. \quad (30)$$

Next, the second term can be expanded by $|\mathcal{Z}| |\mathcal{Z}|^{-1}$, yielding

$$= \frac{1}{\mu} \mathbb{E}_{\substack{\mathbf{z}_t \sim p(\mathbf{z}_t) \\ \tilde{\mathbf{z}}_t \sim p(\tilde{\mathbf{z}}_t | \mathbf{z}_t)}} [\delta(h(\tilde{\mathbf{z}}_t), h(\mathbf{z}_t))] \quad (31)$$

$$+ \mathbb{E}_{\mathbf{z}_t \sim p(\mathbf{z}_t)} \left[\log \left(\int_{\mathcal{Z}} \frac{|\mathcal{Z}|}{|\mathcal{Z}|} e^{-\delta(h(\tilde{\mathbf{z}}_t), h(\mathbf{z}_t)) / \mu} d\tilde{\mathbf{z}}_t \right) \right]. \quad (32)$$

Finally, by using asymptotics of $\mathcal{L}_{\text{contr}}$ derived by [Wang and Isola, 2020] and the marginal is uniform, i.e., $p(\tilde{\mathbf{z}}_t) = |\mathcal{Z}|^{-1}$,

this can be simplified as

$$= \frac{1}{\mu} \mathbb{E}_{\substack{\mathbf{z}_t \sim p(\mathbf{z}_t) \\ \tilde{\mathbf{z}}_t \sim p(\tilde{\mathbf{z}}_t|\mathbf{z}_t)}} [\delta(h(\tilde{\mathbf{z}}_t), h(\mathbf{z}_t))] \quad (33)$$

$$+ \mathbb{E}_{\mathbf{z}_t \sim p(\mathbf{z}_t)} \left[\log \left(\mathbb{E}_{\tilde{\mathbf{z}}_t \sim p(\tilde{\mathbf{z}}_t)} \left[e^{-\delta(h(\tilde{\mathbf{z}}_t), h(\mathbf{z}_t))/\mu} \right] \right) \right] \quad (34)$$

$$+ \log |\mathcal{Z}|. \quad (35)$$

$$= \lim_{M \rightarrow +\infty} \mathcal{L}_{\text{contr}}(r; \mu, M) - \log M + \log p|\mathcal{Z}|. \quad (35)$$

□

Theorem 1 (Minimizers of cross-entropy recover the latent variables and their relations). *Let latent space \mathcal{Z} be a convex body in \mathbb{R}^d , $h = r \circ g : \mathcal{Z} \mapsto \mathcal{Z}$, f be a causal transition function, and δ be a metric, induced by a norm. If g is differentiable and injective, r, f are expressive enough to be minimizers of contrastive objective $\mathcal{L}_{\text{contr}}$ in Eq. (5) for $M \rightarrow +\infty$, then, we have $h = r \circ g$ is invertible and affine mapping and f captures the ground-truth causal relations.*

Proof. According to the Lemma 1, once the positive pairs are given by $\tilde{\mathbf{z}}_t = f(\mathbf{z}_{H_t}, \epsilon_t)$, the cross-entropy between the conditional distribution p and $q_{h,f}$ is given by,

$$\lim_{M \rightarrow +\infty} \mathcal{L}_{\text{contr}}(r, f; \mu, M) - \log M + \log |\mathcal{Z}| = \mathbb{E}_{\mathbf{z}_t \sim p(\mathbf{z}_t)} [H(p(\cdot|\mathbf{z}_t), q_{h,f}(\cdot|\mathbf{z}_t))], \quad (36)$$

Note that $q_{h,f}(\tilde{\mathbf{z}}_t|\mathbf{z}_t)$ is powerful enough to match $p(\tilde{\mathbf{z}}_t|\mathbf{z}_t)$ for the correct choice of h and f on any point \mathbf{z}_t , e.g., the isometry. If h and f is minimizers of the cross-entropy $\mathbb{E}_{p(\tilde{\mathbf{z}}_t|\mathbf{z}_t)} [-\log q_{h,f}(\tilde{\mathbf{z}}_t|\mathbf{z}_t)]$, then we have

$$p(\tilde{\mathbf{z}}_t|\mathbf{z}_t) = q_{h,f}(\tilde{\mathbf{z}}_t|\mathbf{z}_t). \quad (37)$$

The distance metric $\delta(\cdot, \cdot)$ used in the prior conditional distribution p and parameterized conditional distribution $q_{h,f}$:

$$p(\tilde{\mathbf{z}}_t|\mathbf{z}_t) = q_{h,f}(\tilde{\mathbf{z}}_t|\mathbf{z}_t) \quad (38)$$

$$\Leftrightarrow C_p^{-1}(\mathbf{z}_t) e^{-\delta(\tilde{\mathbf{z}}_t, \mathbf{z}_t)} = C_h^{-1}(\mathbf{z}_t) e^{-\delta(h(\tilde{\mathbf{z}}_t), h(\mathbf{z}_t))/\mu} \quad (39)$$

$$\Leftrightarrow C_p(\mathbf{z}_t) = C_h(\mathbf{z}_t). \quad (40)$$

By expanding the formulation of f with the parametric causal transition as:

$$f(\mathbf{z}_{H_t}, \epsilon_t) = \sum_{\tau=1}^L \mathbf{A}_\tau \mathbf{z}_{t-\tau} + \epsilon_t, \quad (41)$$

and take it into the definition of conditional distribution:

$$p(\tilde{\mathbf{z}}_t|\mathbf{z}_t) = C_p^{-1}(\mathbf{z}_t) e^{-\delta(\tilde{\mathbf{z}}_t, \mathbf{z}_t)} \quad (42)$$

$$= C_p^{-1}(\mathbf{z}_t) e^{-\delta(f(\mathbf{z}_{H_t}), \mathbf{z}_t)}, \quad (43)$$

similarly, the definition of parameterized conditional distribution is:

$$q_{h,f}(\tilde{\mathbf{z}}_t|\mathbf{z}_t) = C_h^{-1}(\mathbf{z}_t) e^{-\delta(h(\tilde{\mathbf{z}}_t), h(\mathbf{z}_t))/\mu} \quad (44)$$

$$= C_h^{-1}(\mathbf{z}_t) e^{-\delta(f(h(\mathbf{z}_{H_t})), h(\mathbf{z}_t))/\mu}. \quad (45)$$

As the marginal normalization constants are identical, we obtain for all $\mathbf{z}_t \in \mathcal{Z}$

$$e^{-\delta(\tilde{\mathbf{z}}_t, \mathbf{z}_t)} = e^{-\delta(h(\tilde{\mathbf{z}}_t), h(\mathbf{z}_t))/\mu} \quad (46)$$

$$\Leftrightarrow e^{-\delta(f(\mathbf{z}_{H_t}), \mathbf{z}_t)} = e^{-\delta(f(h(\mathbf{z}_{H_t})), h(\mathbf{z}_t))}, \quad (47)$$

then, by the definition of f which is parameterized by a series of full-rank matrices, it is bijective. And $\tilde{\mathbf{z}}_t = f(\mathbf{z}_{H_t})$, hence, $q_{h,f}(\tilde{\mathbf{z}}_t|\mathbf{z}_t) = q_{h,f}(\mathbf{z}_t|\mathbf{z}_{H_t})$ we can derive the conditional distribution as:

$$p(\mathbf{z}_t|\mathbf{z}_{H_t}) = q_{h,f}(\mathbf{z}_t|\mathbf{z}_{H_t}) \quad (48)$$

$$\Leftrightarrow \delta(f(\mathbf{z}_{H_t}), \mathbf{z}_t) = \frac{1}{\mu} \delta(f(h(\mathbf{z}_{H_t})), h(\mathbf{z}_t)) \quad (49)$$

$$\Leftrightarrow \|\epsilon_t\|_\alpha = \frac{1}{\mu} \|h(\epsilon_t)\|_\alpha. \quad (50)$$

This means that h preserves the ℓ_α -distance between points. Moreover, because h is bijective, the Mazur-Ulam theorem tells us that h must be an affine transform, i.e., by choosing proper μ , there is an orthogonal matrix $\mathbf{U} \in \mathbb{R}^{d \times d}$ that $h(\epsilon_t) = \mathbf{U}\epsilon_t$ and $h(\mathbf{z}_t) = \mathbf{U}\mathbf{z}_t$. Define the delay operator $z^{-\tau}$, and extend the multichannel blind deconvolution from

$$\epsilon_t = \mathbf{z}_t - \tilde{\mathbf{z}}_t = \left[\mathbf{I} - \sum_{\tau=1}^L \mathbf{A}_\tau z^{-\tau} \right] \mathbf{z}_t \quad (51)$$

take $\mathbf{z}_t = \mathbf{U}^\top h(\mathbf{z}_t)$ and exchange the ϵ_t and \mathbf{z}_t in Eq. (51), then, by extending [Zhang and Hyvärinen, 2011, Lemma 1] we have following equivalence:

$$\mathbf{z}_t = \left[\left(\mathbf{I} - \sum_{\tau=1}^L \mathbf{A}_\tau z^{-\tau} \right)^{-1} \right] \epsilon_t \quad (52)$$

$$= \mathbf{U}^\top \left[\left(\mathbf{I} - \sum_{\tau=1}^L \mathbf{U} \mathbf{A}_\tau \mathbf{U}^\top z^{-\tau} \right)^{-1} \right] h(\epsilon_t) \quad (53)$$

$$= \left[\left(\mathbf{I} - \sum_{\tau=1}^L \mathbf{A}_\tau z^{-\tau} \right)^{-1} \right] \mathbf{U}^\top h(\epsilon_t). \quad (54)$$

Note, this result is consistent with that h must be an affine transform, i.e., there is an orthogonal matrix making the estimated source be $h(\mathbf{z}_t) = \mathbf{U}\mathbf{z}_t$ and the estimated transition matrix $\hat{\mathbf{A}}_\tau = \mathbf{A}_\tau \mathbf{U}^\top$. In other words, once the minimizers of contrastive loss $\mathcal{L}_{\text{contr}}$ are obtained, the identifiability is guaranteed up to linear equivalence classes, and any solution within them is the best solution. □

Further, by choosing proper $\delta(\cdot, \cdot)$, the results extended from Banach-Lamperti Theorem [Lamperti, 1958] indicate that we can achieve a more strong identifiability:

Theorem C.1. *For non-isotropic norm induced metric ℓ_α , if $1 \leq \alpha \leq \infty$ and $\alpha \neq 2$. A matrix $\mathbf{U} \in \mathbb{R}^{d \times d}$ is an isometry if and only if \mathbf{U} is a generalized permutation matrix, there is only a channel permutation π between estimations and ground-truth such that $\hat{z}_{i,t} = s_i z_{\pi(i),t}$, where s_i is a scaling constant.*

Proof. See [Li and So, 1994]. □

C.3 Proof of Theorem 2

Theorem 2 (Minimizers of the multi-view objective maintains the channel correspondency). *Let $\mathcal{Z}^v \subseteq \mathbb{R}^{d_v}$, $\mathcal{Z} = \cup \mathcal{Z}^v$ and $\cap \mathcal{Z}^v \neq \emptyset$. If $\mathbf{B}^v \in \mathfrak{B}_{d_v}$ be a doubly stochastic matrix, $r, f, \{\mathbf{B}^v\}$ are the minimizers of contrastive objective for $M \rightarrow +\infty$, then, we have $h = r \circ g$ is an isometry, and $\{\mathbf{B}^v\}$ can rearrange the components of each view source such that common components from each view source are aligned.*

Proof. Since the source \mathbf{z}_t^v of each view is first recovered by a reverse function r^v individually, there is a distinctive transformation h^v between each estimated view-specific source $\hat{\mathbf{z}}_t^v$ and true \mathbf{z}_t^v . We show that if and only if the Eq. (11) is optimized, the $r, f, \{\mathbf{B}^v\}$ are minimizers of the contrastive objective. Before continuing, we first show the property of a doubly stochastic matrix \mathbf{B}^v . By Birkhoff–von Neumann theorem, a doubly stochastic matrix can be represented by

$$\mathbf{B}^v = \theta_1 \mathbf{P}_1^v + \dots + \theta_k \mathbf{P}_k^v, \quad (55)$$

where $\theta_1, \dots, \theta_k \geq 0$ and $\sum_{i=1}^k \theta_i = 1$, and permutation matrix $\mathbf{P}_i^v \in \{0, 1\}^{d_v \times d_v}$.

Therefore, $R(\mathbf{B}^v)$ is non-negative, and the minimizers of

$$\sum_{v=1}^2 \mathbb{E} [\|(\mathbf{B}^v \mathbf{z}_t^v)_{1:d_c} - \mathbf{c}_t^*\|^2] + \eta R(\mathbf{B}^v),$$

can only be obtained by enforcing both the first and second terms to be zero. The first term is achieved when $(\mathbf{B}^v \hat{\mathbf{z}}_t^v)_{1:d_c} = \mathbf{c}_t^*$ for all views, and the second term is achieved when \mathbf{B}^v converges to a permutation matrix such that $R(\mathbf{B}^v) = -\sum_{i,j} B_{i,j} \log B_{i,j} = 0$.

Then, the common source estimated from different views differ in a permutation transformation, i.e., a channel rearrangement,

$$(\mathbf{P}^1 \hat{\mathbf{z}}_t^1)_{1:d_c} = (\mathbf{P}^2 \hat{\mathbf{z}}_t^2)_{1:d_c} = \mathbf{c}_t^*. \quad (56)$$

If \mathbf{c}_t^* was not the common source, there would be some components of private source entangled in \mathbf{c}_t^* that are equivalent on every point. This would mean that these components are actually same on all points, which contradicts the assumption that \mathbf{c}_t^* is not the common source.

Further, this result also indicates that the common source and the private source are disentangled, thereby the merge operator that splits and re-concatenates the estimated sources to construct the complete source is guaranteed to be consistent with the optimal condition. \square

By the Theorem 1 h is an affine transformation and the common source and the private sources are disentangled. For a source that generates two views, there is an orthogonal matrix \mathbf{U} such that:

$$\hat{\mathbf{z}}_t = \mathbf{U} \mathbf{z}_t \quad (57)$$

$$= \begin{bmatrix} \mathbf{U}_c & \mathbf{0} & \mathbf{0} \\ \mathbf{0} & \mathbf{U}_1 & \mathbf{0} \\ \mathbf{0} & \mathbf{0} & \mathbf{U}_2 \end{bmatrix} \begin{bmatrix} \mathbf{c}_t \\ (\mathbf{B}^1 \mathbf{z}_t^1)_{d_c+1:d_1} \\ (\mathbf{B}^2 \mathbf{z}_t^2)_{d_c+1:d_2} \end{bmatrix}, \quad (58)$$

where $\mathbf{U}_c \in \mathbb{R}^{d_c \times d_c}$, $\mathbf{U}_1 \in \mathbb{R}^{d_1-d_c \times d_1-d_c}$ and $\mathbf{U}_2 \in \mathbb{R}^{d_2-d_c \times d_2-d_c}$ are orthogonal matrices. Moreover, when ℓ_α is non-isotropic norm induced metric, the $\mathbf{U}_c, \mathbf{U}_1$ and \mathbf{U}_2 can also be narrowed down to the permutation matrices.

D Practical Implementations

In this section, we describe the details of the practical implementation of more experiments. All experiments are conducted on two workstations with 8 NVIDIA RTX 2080Ti GPUs.

D.1 Handle More Views

As mentioned, the MuLTI can be easily extended to more than 2 views. Herein, we conduct experiments on **Multi-view VAR** dataset under different numbers of views $V \in \{1, 2, 3, 4\}$, we set the dimensions of ground-truth latent variables to $d = 10$, time lags to $L = 2$, noise distribution follow the Laplacian with $\lambda = 0.05$. Setting details for each scenario are as follows:

$$V = 1 : d_c = d = 10$$

$$V = 2 : d_c = 4, d_1 = 7, d_2 = 7$$

$$V = 3 : d_c = 4, d_1 = 6, d_2 = 6, d_3 = 6$$

$$V = 4 : d_c = 2, d_1 = 4, d_2 = 4, d_3 = 4, d_4 = 4$$

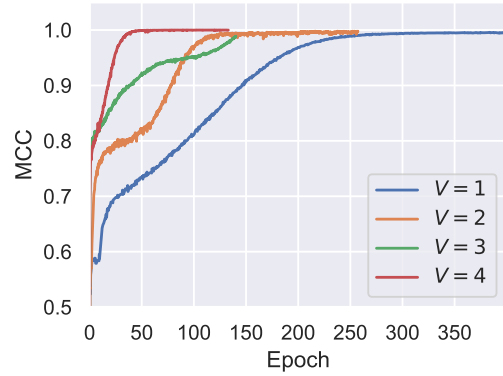


Figure D.1: MCC trajectories with different numbers of views.

In the case of $V = 1$, no further merge operation is required; therefore, the permutation learning module is removed. According to the results, MuLTI achieves full identifiability in all scenarios, thus MuLTI can handle datasets with more than two views successfully.

D.2 Handle Higher Dimension

We would like to add the results larger than the general setting, by setting 40% dimensions to be shared, $d=10, 16, 20, 50$. The results are shown in Table D.1.

Table D.1: Ablation results with higher dimension

Source Dimension	$d = 10$	$d = 16$	$d = 20$	$d = 50$
MCC	99.80	99.90	99.92	96.58

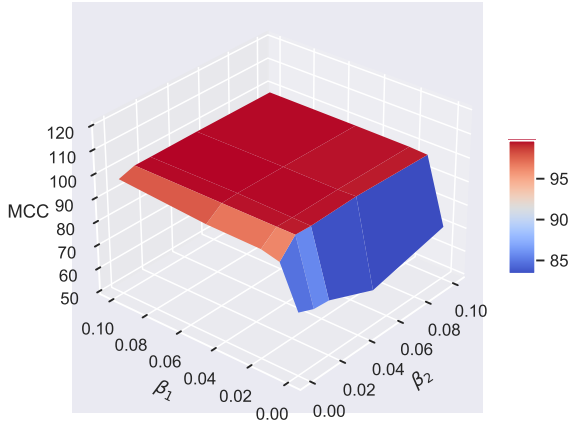


Figure D.2: Results of grid hyper-parameter β_1, β_2 evaluation.

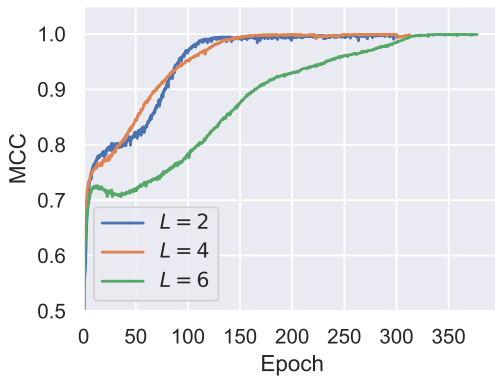


Figure D.3: MCC trajectories with different time lags.

D.3 More Ablation Results

Effect of hyper-parameter

The hyper-parameters for loss include β_1, β_2 , and β_3 , which are weights of each term in the augmented total objective. While the effects of β_1, β_2 are rather obvious than β_3 , we perform a grid search evaluation strategies on $\beta_1 \in \{0.0, 0.01, 0.02, 0.05, 0.1\}, \beta_2 \in \{0.0, 0.01, 0.02, 0.05, 0.1\}$. The results are reported in Figure D.2. The final MCC scores are typically around 99.0%, indicating that model performance is fairly robust to choices of β_1, β_2 . But, when β_1 or β_2 is set to 0, we observe the performance drops notably, which indicates the importance of our residual minimization and merge operations.

Effect of different causal transition time lags

We verify the robustness of our MuLTI under different time lags $L \in \{2, 4, 6\}$ with $\beta_1 = 0.01, \beta_2 = 0.01, \beta_3 = 1e - 5$. The results are shown in Figure D.3. From the results, we can see that although the model takes more steps when the total time lags are $L = 6$, the final result shows that our method can achieve full identifiability in these different experimental scenarios.

D.4 Time Complexity

It is true that the original OT algorithm suffers from a high time complexity problem, however, the Sinkhorn algorithm can be efficiently implemented on GPUs. We clock the experiments with different D sizes [10, 20, 50], and the total running time of Sinkhorn/complete training of 800 epochs are shown in Table D.2. It can be shown that the Sinkhorn iterations take less than 1/10 time cost that regular model training.

Table D.2: Total running time (in hours) of the Sinkhorn-Knopp iterations and model training on GPUs.

Source Dimension	d=10	d=20	d=50
Sinkhorn-Knopp	0.30	0.69	0.89
Model Training	3.31	6.71	8.81

D.5 Details of Datasets Configuration

Synthetic VAR

is a synthetic dataset modified from [Yao *et al.*, 2021], which involves VAR processes and corresponding nonlinear multi-view observations. To generate latent process, we first select transition matrices $\{A_\tau\}_{\tau=1}^L$ from uniform distribution $U[-0.5, 0.5]$, then sample initial states $\{z_t\}_{t=1}^L$ from normal distribution for generating sequences $\{z_t\}_{t=1}^T$. To generate multi-view time series, we randomly select d_1 and d_2 dimensions of latent variables for each view. The nonlinear observations of each view are created by mixing latent variables with random parameterized MLPs $g^v(\cdot)$ following previous work [Hyvärinen and Morioka, 2017]. Specifically, each $g^v(\cdot)$ is composed of three hidden fully connected layers and Leaky ReLU units.

Mass-spring system

is a classical physical system that follows Hooke’s law. In this dataset, eight balls are simulated inside a 2D box where they may collide elastically with its walls. A spring is connected to each pair of variables with a uniform probability.

$$f_{ij} = -\Delta_k (\mathbf{y}_i - \mathbf{y}_j), \quad \dot{\mathbf{y}}_i = \sum_{j=1}^N f_{ij}, \quad \mathbf{p}_i = \{\mathbf{y}_i, \dot{\mathbf{y}}_i\}$$

The f_{ij} represents the unidirectional interaction between a ball j and a ball i , with Δ_k denoting the type of edge for each pair of variables, and \mathbf{y}_i and $\dot{\mathbf{y}}_i$ denoting the ball’s 2D position and velocity, respectively. The continuous variable \mathbf{p}_i is constructed by concatenating the position and the velocity. A step-by-step integration of the previous differential equations is used to simulate the trajectory once the initial location and velocity have been sampled. Trajectories are obtained by sub-sampling every 50 steps at a step size of 0.001. In practice, we create the scenario of simulation and generate the trajectories with *Pymunk*, then render the trajectories into two views with *Matplotlib*. We set the rest length of the spring to [5, 10], and we set the stiffness of the spring in relation to 20. Additionally, external forces are added to the ball at each time step, which are sampled from a Laplacian noise distribution with $\lambda = 0.1$.

D.6 Pseudo-Code of MuLTI

We summarize the pseudo-code of our MuLTI method in Algorithm 1.

Algorithm 1 Pseudo-code for MuLTI

Input: Training dataset $\{\mathcal{X}^v\}$, encoders $\{r^v\}$, transition function f , matrices $\{B^v\}$.

Parameter: $\beta_1, \beta_2, \beta_3, \mu, \eta$

Output: Trained encoders $\{r^v\}$, transition functions f , permutation matrices B^v .

```

1: Let  $t = 0$ ;
2: while Not converge do
3:   Sample a mini-batch  $\{\mathbf{x}^v\}$ ;
4:   Obtain  $\{\mathbf{z}_t^v = r^v(\mathbf{x}_t^v)\}$ ;
5:   Merge  $\mathbf{z}_t = \mathbf{m}(\{\mathbf{z}_t^v\})$  from each  $\{\mathbf{z}_t^v\}$ ;
6:   Construct  $\{(\mathcal{H}_t, \mathbf{z}_t)\}$  from  $\{\mathbf{z}_t\}$ ;
7:   Fetch causal transited variable  $\tilde{\mathbf{z}}_t = f(\mathcal{H}_t)$ ;
8:   Construct contrastive pairs  $(\mathbf{z}_t, \tilde{\mathbf{z}}_t), (\mathbf{z}_t, \mathbf{z}_t^-)$ ;
9:   Obtain  $\{\hat{\epsilon}_{i,t}\}$  and  $\{\hat{\epsilon}_{i,t}\}^{\text{perm}} = \text{randperm}(\{\hat{\epsilon}_{i,t}\})$ ;
10:  if Do contrastive learning then
11:    Compute  $\mathcal{L}_{\text{contr}}$  according to Eq.(5);
12:     $\mathcal{L}_\epsilon = \mathbb{E}_{\{(\mathbf{z}_t, \tilde{\mathbf{z}}_t)\}} \delta(\mathbf{z}_t, \tilde{\mathbf{z}}_t)$ ;
13:     $\mathcal{L}_m = \sum_v \mathbb{E}[\|(\mathbf{B}^v \mathbf{z}_t^v)_{1:D_c} - \mathbf{c}_t^*\|^2]$ ;
14:     $\mathcal{L}_D = \log \mathcal{D}(\{\hat{\epsilon}_{i,t}\}) - \log(1 - \mathcal{D}(\{\hat{\epsilon}_{i,t}\}^{\text{perm}}))$ ;
15:     $\mathcal{L} = \mathcal{L}_{\text{contr}} + \beta_1 \mathcal{L}_m + \beta_2 \mathcal{L}_\epsilon + \beta_3 \mathcal{L}_D$ ;
16:    Minimize loss  $\mathcal{L}$ ;
17:  else if Do permutation learning then
18:     $\mathcal{L}_m = \sum_v \mathbb{E}[\|(\mathbf{B}^v \mathbf{z}_t^v)_{1:D_c} - \mathbf{c}_t^*\|^2] + \eta R(\mathbf{B}^v)$ ;
19:    Minimize loss  $\mathcal{L}_m$ ;
20:  else if Do discriminator learning then
21:     $\mathcal{L}'_D = \log \mathcal{D}(\{\hat{\epsilon}_{i,t}\}) + \log(1 - \mathcal{D}(\{\hat{\epsilon}_{i,t}\}^{\text{perm}}))$ ;
22:    Minimize loss  $\mathcal{L}'_D$ ;
23:  end if
24: end while
25: return  $\{r^v\}, \{B^v\}, f, \{\mathbf{z}_t\}$ .

```

Appendix References

- [Hyvärinen and Morioka, 2017] Aapo Hyvärinen and Hiroshi Morioka. Nonlinear ICA of temporally dependent stationary sources. In *Proc. of AISTATS*, 2017.
- [Kuhn, 1955] Harold W Kuhn. The Hungarian method for the assignment problem. *Naval research logistics quarterly*, 1955.
- [Lamperti, 1958] John Lamperti. On the isometries of certain function-spaces. *Pacific Journal of Mathematics*, 1958.
- [Li and So, 1994] Chi-Kwong Li and Wasin So. Isometries of p-norm. *The American Mathematical Monthly*, 1994.
- [Wang and Isola, 2020] Tongzhou Wang and Phillip Isola. Understanding contrastive representation learning through alignment and uniformity on the hypersphere. In *Proc. of ICML*, 2020.
- [Yao *et al.*, 2021] Weiran Yao, Yuewen Sun, Alex Ho, Changyin Sun, and Kun Zhang. Learning Temporally Causal Latent Processes from General Temporal Data. In *Proc. of ICLR*, 2021.
- [Zhang and Hyvärinen, 2011] Kun Zhang and Aapo Hyvärinen. A General Linear Non-Gaussian State-Space Model: Identifiability, Identification, and Applications. In *Proc. of ACML*, 2011.
- [Zimmermann *et al.*, 2021] Roland S. Zimmermann, Yash Sharma, Steffen Schneider, Matthias Bethge, and Wieland Brendel. Contrastive learning inverts the data generating process. In *Proc. of ICML*, 2021.